

Research Article

Open Access



Extended fault-pair Boolean table based test points selection for robotic systems

Xiuli Wang^{1,2}, Dongdong Xie¹, Yang Li³, Jun Tian², Kai Li⁴

¹College of Information Engineering, Zhejiang University of Technology, Hangzhou 310023, Zhejiang, China.

²College of Software, Nankai University, Tianjin 300350, China.

³School of Mechatronic Engineering and Automation, Shanghai University, Shanghai 200444, China.

⁴Jiaxing New Jies Heat & Power Co., Ltd., Jiaxing 314016, Zhejiang, China.

Correspondence to: Dr. Yang Li, School of Mechatronic Engineering and Automation, Shanghai University, Shanghai 200444, China. E-mail: yongerli@shu.edu.cn

How to cite this article: Wang, X.; Xie, D.; Li Y.; Tian, J.; Li, K. Extended fault-pair Boolean table based test points selection for robotic systems. *Intell. Robot.* 2025, 5(2), 419-32. <http://dx.doi.org/10.20517/ir.2025.21>

Received: 31 Dec 2024 **First Decision:** 14 Mar 2025 **Revised:** 7 May 2025 **Accepted:** 9 May 2025 **Published:** 21 May 2025

Academic Editor: Qiang Liu **Copy Editor:** Pei-Yun Wang **Production Editor:** Pei-Yun Wang

Abstract

Analog circuit fault isolation is crucial for ensuring the reliability and performance of robotic systems. Test point selection plays a key role in enabling effective fault isolation, yet traditional methods often struggle to balance the number of test points with fault isolation accuracy. This paper proposes a novel test point selection method by extending the fault-pair Boolean table into a distributional framework. The approach enhances test point selection by employing the Bhattacharyya Coefficient to quantify distributional overlap and using kernel density estimation (KDE) to model circuit response distributions without assuming normality. To further improve estimation accuracy, the Grey Wolf optimization algorithm is applied for optimal KDE bandwidth selection. Experimental results on a negative feedback circuit show that the proposed method successfully isolates all 11 faults, demonstrating strong isolation capability. Further validation on an active filter circuit confirms its effectiveness, achieving successful isolation of 16 out of 20 faults. Compared to other methods, the proposed approach consistently yields higher fault isolation across various thresholds.

Keywords: Robotic systems, analog circuit, fault isolation, fault-pair Boolean table, kernel density estimation, Bhattacharyya coefficient, grey wolf optimization



© The Author(s) 2025. **Open Access** This article is licensed under a Creative Commons Attribution 4.0 International License (<https://creativecommons.org/licenses/by/4.0/>), which permits unrestricted use, sharing, adaptation, distribution and reproduction in any medium or format, for any purpose, even commercially, as long as you give appropriate credit to the original author(s) and the source, provide a link to the Creative Commons license, and indicate if changes were made.



1. INTRODUCTION

With the rapid advancements in robotics, internal circuit systems, particularly analog circuits, have become critical components prone to frequent failures due to their nonlinear characteristics and the complexity of operating environments^[1,2]. Research indicates that more than 80% of circuit failures originate from analog circuits, which directly affect the stability and functionality of robotic systems^[3,4]. As a result, efficiently isolating analog circuit faults has emerged as a pivotal challenge in ensuring the reliability of robotic systems. Design for testability (DFT) plays a crucial role in fault diagnosis of analog circuits^[5]. By introducing test points within the circuit to capture critical node signals, DFT significantly enhances the observability of the circuit, thereby improving its fault diagnosability. This approach not only increases test coverage but also effectively reduces fault localization time and lowers maintenance costs. Moreover, the effective implementation of testability design supports real-time condition monitoring, enabling the system to perform self-detection and self-diagnosis during operation, thereby enhancing equipment reliability and maintenance efficiency. However, an excessive number of test points can result in information redundancy, increased system complexity, and elevated testing costs, necessitating optimization of test point selection^[6]. The optimization of test point selection refers to the process of strategically identifying and selecting the most effective set of test points in a system or circuit to achieve accurate fault diagnosis or isolation while minimizing cost, complexity, and redundancy. This process aims to balance the trade-off between diagnostic accuracy and the number of test points^[7].

In recent years, significant research has been conducted on test point selection for analog circuits. Fault dictionary-based approaches to test point selection have emerged as a relatively mature method (with integer coding tables being a specific form of fault dictionary, which will not be differentiated here). A tolerance handling method was proposed in^[8] for diagnosing soft faults in analog circuits, addressing diagnostic inaccuracies caused by component tolerances. This method introduced a slope fault model and combines optimization theory with threshold coefficients, leading to a novel fault dictionary-based test point selection approach. A depth-first graph search-based test point selection method was given in^[9] for analog circuit fault dictionaries, maximizing information gain during the graph node expansion process. This ensures that each additional test point provides the maximum information, facilitating the achievement of a globally minimal test point set. Subsequently, a heuristic graph search approach was proposed by integrating the concept of entropy from information theory and combining fuzzy sets caused by component tolerances with fault voltage distributions in^[10] to evaluate the optimality of test points. A clustering discretization method was applied to overcome the limitations of traditional fault dictionaries in handling component tolerances and continuous-value monitoring variables in^[11]. This method represented fault modes as a set of single or multiple integer codes by introducing an extended fault dictionary. Building on this, an extended integer-coded dictionary method was provided to address fault localization issues in switch-mode power supplies in^[12], utilizing optimal boundary determination techniques to enhance feature separation. To improve the computational efficiency of fault dictionaries, an efficient test point selection method was proposed in^[13] that optimizes the test point set by progressively eliminating isolated faults and test points, thereby resolving the issues of excessive computation time and high dimensionality encountered in traditional approaches.

The above analog circuit test point selection algorithms are all based on fault dictionary technology. However, fault dictionary technology is not a highly precise method. When the number of test points increases, not only does the diagnostic accuracy decrease, but the computational complexity also increases. A more precise fault pair Boolean table technique was proposed in^[14,15], overcoming the limitations of traditional integer-coded table techniques, which cannot isolate all faults. The fault pair Boolean table is constructed based on node voltage values. For two faults, if the voltage difference at the same test point exceeds a given threshold^[16], the two faults are considered isolable, and the corresponding position is marked as 1. Otherwise, if the voltage difference is smaller than the threshold, the faults are deemed non-isolable, and the corresponding position is marked as 0. The given threshold involves a degree of subjectivity and lacks general applicability. Thus, an

ambiguity model based on the normal distribution assumption was proposed using the overlap area between probability density curves as a criterion for judgment in [17]. Considering the diversity of sample distributions, a kernel density estimation (KDE) as a substitute for the aforementioned normal distribution was presented in [15], offering a more practical approach. However, [17] and [18] are still considered as extensions of the fault dictionary technique, which limits the effectiveness of the methods. To improve and overcome the shortcomings of existing approaches, [19] combined the concept of fault pairs with the ambiguity gap calculation method, defining a new approach for calculating the fault pair isolation capability at test points. Based on this, a new test point selection method was developed using the fault pair isolation table. Subsequently, a new similarity coefficient criterion was put forward to determine fault isolation degree in [20], taking into account the fact that component tolerance circuit output responses approximately follow a normal distribution.

The methods in [19] and [20] can effectively improve isolation accuracy and select more reasonable test points. However, they assume that circuit output responses follow a normal distribution, which may not hold in real-world scenarios. In real-world scenarios, fault data often originate from heterogeneous devices or distributed sensors, resulting in significant distribution shifts due to measurement deviations, environmental noise, and varying operating conditions. To address this issue, federated transfer learning (FTL) has emerged as a promising solution. By enabling cross-domain knowledge transfer through encrypted parameter exchange, FTL eliminates the need for sharing raw data. For example, Yang *et al.* proposed a targeted transfer learning framework based on distribution barycenter mediation (TTL-DBM) [21]. This approach employs optimal transport theory to construct the Wasserstein barycenter between the source and target domains as an intermediary, and dynamically aligns marginal and conditional distributions via federated learning. The method achieved high-precision feature adaptation under decentralized data conditions in mechanical fault diagnosis, demonstrating the effectiveness of distribution alignment strategies in complex system diagnostics. This provides important insights for analog circuit fault diagnosis: by adopting non-parametric distribution modeling, it is possible to overcome the limitations of traditional methods that rely on specific distribution assumptions, thereby enhancing diagnostic robustness in complex environments. Therefore, this paper proposes a novel test point selection method that employs the Bhattacharyya coefficient (BC) to quantify distribution overlap and utilizes KDE to model circuit output responses. This approach eliminates the dependence on specific distribution assumptions, making test point selection more general and adaptable to complex environments. The BC measures the similarity between probability distributions by calculating the overlap between two distributions, which enhances fault distinguishability and improves fault isolation accuracy. Meanwhile, KDE, as a non-parametric probability density estimation method, models circuit output distributions without assuming a specific distribution form. This allows the proposed method to accommodate a broader range of data distributions beyond the traditional normal distribution assumption, enhancing its applicability and flexibility in real-world circuit testing scenarios. The main contributions of this paper are as follows.

1. The BC is utilized to calculate overlap areas, replacing the traditional distance computations based on individual samples in fault-pair Boolean tables. This distribution-based approach effectively mitigates inaccuracies arising from reliance on single sample calculations.
2. KDE is employed to model the data distribution in fault-pair Boolean tables, eliminating the traditional normal distribution assumption and providing a more flexible and accurate distribution estimation.
3. The Grey Wolf optimization (GWO) algorithm is utilized to estimate the bandwidth parameter in KDE, achieving a globally optimal solution and ensuring the adaptability and accuracy of KDE across various datasets.

The remaining sections are organized as follows. A BC inspired fault-pair Boolean table is established in Section 2. Then, KDE is stated for KDE approximation and bandwidth is estimated by the GWO algorithm in Section 3. Section 4 gives a whole process of test point selection based on the extended fault-pair Boolean table. Finally, a conclusion is drawn in Section 5.

2. FAULT-PAIR BOOLEAN TABLE ESTABLISHMENT

In this section, the BC is incorporated to improve the fault isolation capability of the fault-pair Boolean table. Firstly, a fault-pair Boolean table is created for fault isolation. Then, the BC is applied to calculate the values within the table.

2.1. Fault-pair Boolean table

A fault-pair Boolean table is essentially a tabular representation of the fault pair-to-test relationship matrix. Each row represents a potential fault pair combination, while each column corresponds to an available test point. The value at each cell indicates the ability of the test point to distinguish between the respective fault pairs.

Let the set of possible faults in the system be denoted as $F = \{f_0, f_1, \dots, f_m\}$, where f_i ($i = 0, 1, 2, \dots, m$) represents the i th fault mode, m is the total number of fault modes, and f_0 represents the fault-free state. All test points are given as $T = \{t_1, t_2, \dots, t_n\}$, where t_j ($j = 1, 2, \dots, n$) corresponds to the j -th test point, and n is the total number of test points. There are $C_{m+1}^2 = m(m+1)/2$ fault pairs, expressed by the set $P = \{p_1, p_2, \dots, p_{C_{m+1}^2}\}$. The fault-to-test point response feature set is denoted as $\mathbf{S} = \{\mathbf{S}_{kj}\}$, where $k = 0, 1, 2, \dots, m$ indicates the fault sample index, and $j = 1, 2, \dots, n$ signifies the test point index. Here, $\mathbf{S}_{kj} = [S_{kj}^1, S_{kj}^2, \dots, S_{kj}^t]$ is the response feature vector of fault k at test point j , containing t feature values. The values in the fault-pair Boolean table are symbolized as $I = \{I_{ij}\}$, where $i = 1, 2, \dots, C_{m+1}^2$ is the fault pair index. Each test point t_j corresponds to column values $\mathbf{t}_j = \{I_{1j}, I_{2j}, \dots, I_{C_{m+1}^2 j}\}$ containing C_{m+1}^2 elements. The determination of I_{ij} is defined by

$$I_{ij} = \begin{cases} 0, & \text{if } t_j \text{ cannot isolate the } i\text{-th pair of fault;} \\ 1, & \text{if } t_j \text{ can isolate the } i\text{-th pair of fault.} \end{cases} \quad (1)$$

The ability of test point t_j to isolate fault pairs depends on the distance between the fault-to-test point response feature vectors. The L_2 -norm is commonly used to quantify this distance, as given in

$$d(f_u, f_v) = \begin{cases} \|\mathbf{S}_{uj} - \mathbf{S}_{vj}\|_2, & u \neq v; \\ 0, & u = v. \end{cases} \quad (2)$$

If the distance between two faults at test point t_j exceeds a certain threshold, the faults can be isolated by the test point t_j ; otherwise, they cannot be isolated.

2.2. Fault-pair Boolean table based on BC

The distance in Equation (2) is initially calculated based on a single sample. This single-sample approach doesn't fully capture the underlying variations in the data, potentially resulting in incorrect fault isolation. To overcome this limitation, the BC is employed to calculate the overlap area between different distributions derived from multiple samples^[22–24]. The BC is expressed as

$$BC(f_u, f_v) = \int \sqrt{p_u(x) p_v(x)} dx \quad (3)$$

where $p_u(x)$ and $p_v(x)$ denote the corresponding probability density distributions of fault f_u and f_v , respectively. The value of the BC ranges from 0 to 1. When $p_u(x) = p_v(x)$, $BC = 1$. Then, Equation (2) can be modified based on the BC as follows.

$$d(f_u, f_v) = 1 - BC(f_u, f_v) \quad (4)$$

which is further illustrated in Figure 1. As given in Figure 1A, if $d = 1$, then f_u and f_v are completely separable. In Figure 1B, if $d = 0$, that is the curves of $p_u(x)$ and $p_v(x)$ almost overlap, then f_u and f_v cannot be separated. In Figure 1C, if $0 < d < 1$, then f_u and f_v are partially separable.

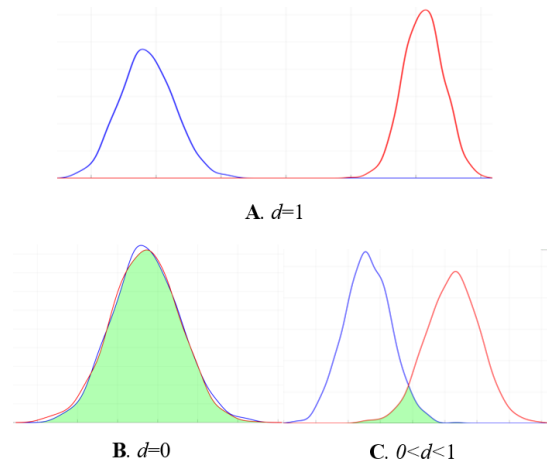


Figure 1. The curves of probability density function $p_u(x)$ and $p_v(x)$. (A) The distribution of fault f_u and fault f_v corresponds to no overlap, and fault f_u and fault f_v can be completely separated; (B) The distributions corresponding to fault f_u and fault f_v overlap completely, and fault f_u and fault f_v cannot be separated; (C) The distributions corresponding to fault f_u and fault f_v overlap partially, and fault f_u and fault f_v can be partially separated.

Based on the fault-pair Boolean table derived using BC, if the values calculated by Equation (4) between two faults at a given test point t_j exceed a certain threshold ε within the range $[0, 1]$, the faults can be isolated at that test point; otherwise, they cannot be isolated.

3. BC APPROXIMATION VIA KDE

The probability density function in Equation (4) is unknown in the circuits of robotic systems. Typically, it is assumed to follow a specific probability distribution for inference, which introduces subjectivity. To address this situation, this paper applies KDE to infer the probability density function from available samples [25,26]. Let $X_u^j = (x_{u,1}^j, x_{u,2}^j, \dots, x_{u,q}^j)$ be q random samples collected from test point t_j ($j = 1, 2, \dots, n$). The probability density function $p_u(x)$ ($u = 0, 1, 2, \dots, m$) of fault f_u at test point t_j can be derived by the KDE as:

$$\widehat{p}_u(x) = \frac{1}{qh} \sum_{i=1}^q K\left(\frac{x - x_{u,i}^j}{h}\right) \quad (5)$$

where h is a bandwidth parameter, K is the kernel function and $\int K(x) dx = 1$.

As is noted that the bandwidth h plays a key role in KDE for determining the smoothness of the estimate. A bandwidth that is too small results in an estimate that is overly 'rough', whereas a bandwidth that is too large may excessively smooth the data, causing important details to be overlooked [27]. Therefore, an appropriate bandwidth is crucial for ensuring an accurate approximation of BC. The GWO, a global optimization method simulating the hunting behavior of grey wolves [28], is adopted to estimate the bandwidth parameter.

The GWO has very few parameters, and the initial search does not require any derivation information. Gray wolves are typically classified into four types: α wolves, β wolves, δ wolves, and ω wolves. The α wolf is the leader of the pack, responsible for guiding the group in hunting prey. In optimization algorithms, the α wolf represents the optimal solution. β wolves assist the α wolf and correspond to the second-best solutions in the algorithm. δ wolves follow the commands and decisions of the α and β wolves, playing the role of scouts and guardians for the pack. Wolves with lower fitness levels may be demoted from α or β to the δ level. ω wolves are the lowest-ranking wolves, following the actions of the higher-ranking wolves.

Gray wolves gradually approach and encircle their prey. The following update equation is proposed to model this behavior.

$$U(t+1) = U_P(t) - A \cdot |C \cdot U_P(t) - U(t)| \quad (6)$$

where $U(t+1)$ denotes the position of the gray wolf at time $t+1$; $U(t)$ represents the position of the gray wolf at time t ; U_P denotes the position of the prey; A and C are two synergy coefficient vectors, which are further expressed by

$$A = 2a \cdot r_1 - a \quad (7)$$

$$C = 2 \cdot r_2 \quad (8)$$

where a is a vector and its components are linearly decreased from 2 to 0 over iterations; r_1 and r_2 are random variables in $[0, 1]$.

To further simulate the hunting behavior of grey wolves, it is assumed that α , β , and δ possess strong capabilities to identify the position of potential prey. During each iteration, the best three wolves (α , β , and δ) in the current population are retained, and the positions of ω are updated based on the position information of these top three wolves. Therefore, the wolves of ω should be obliged to update their positions as follows:

$$U(t+1) = \frac{(U_1(t+1) + U_2(t+1) + U_3(t+1))}{3} \quad (9)$$

where $U_1(t+1)$, $U_2(t+1)$, $U_3(t+1)$ denote the step sizes and directions that the ω moves towards α , β , and δ at time $t+1$, respectively. They are derived by

$$\begin{aligned} U_1(t+1) &= U_\alpha(t) - A_1 |C_1 \cdot U_\alpha(t) - U(t)| \\ U_2(t+1) &= U_\beta(t) - A_2 |C_2 \cdot U_\beta(t) - U(t)| \\ U_3(t+1) &= U_\delta(t) - A_3 |C_3 \cdot U_\delta(t) - U(t)| \end{aligned} \quad (10)$$

where $U_\alpha(t)$, $U_\beta(t)$, and $U_\delta(t)$ represent the positions of the α , β , and δ at time t , respectively; the A_1 , A_2 , and A_3 denote random vectors inferred by Equation (7); the C_1 , C_2 , and C_3 indicate random vectors given in Equation (8).

It is worth noting that the position of U in Equation (9) corresponds to the bandwidth parameter h that requires optimization. The detailed estimation process is thoroughly defined in Algorithm 1.

Algorithm 1 Bandwidth parameter h estimation by GWO.

1. Initialize parameters: population size, maximum number of iterations, and randomly generated parameters a , A and C .
 2. Construct a mean square error (MSE) objective function based on K-fold cross-validation of KDE. The fitness value for each gray wolf is calculated using this objective function. The population is then ranked based on the fitness value. Assign the positions of the best solution, the second-best solution, and the third-best solution in the population to the grey wolves U_α , U_β , and U_δ , respectively.
 3. Calculate the distance of ω gray wolf from α , β , δ gray wolves and update the position according to Equations (9) and (10).
 4. Recalculate the fitness values based on the updated populations. And reupdate the position and fitness of α , β , and δ according to the newly obtained fitness ordering.
 5. When the maximum number of iterations is reached, terminate the optimization process and output the global optimal solution U_α ; otherwise return to step 3.
-

4. TEST POINT SELECTION

4.1. Test point selection algorithm based on the fault-pair isolation table

For each test point $t_j \in T$, the functions $\hat{f}_u(x)$ and $\hat{f}_v(x)$ of fault pair (f_u, f_v) are achieved by Equation (5). Then, the overlapping area between the $\hat{f}_u(x)$ and $\hat{f}_v(x)$ is calculated by Equation (4) and compared to the threshold ε . If the overlapping area exceeds the threshold ε , the fault pair (f_u, f_v) can be isolated by the test point t_j , and a value of 1 is assigned to the corresponding entry in the fault-pair Boolean table. Otherwise, the fault pair cannot be isolated by the test point, and the value is set to 0. This process is repeated for all fault pairs and test points until the fault-pair Boolean table is fully populated.

After the fault-pair Boolean table is constructed, the optimal test points S_{opt} are selected based on the information in the table. First, a new row $NI(t_j)$ is added, where each entry represents the number of fault pairs that a given test point t_j can isolate. Additionally, a new column NT_i is introduced, where each entry indicates the number of test points capable of isolating a specific fault pair. Then, the detailed procedure for selecting test points is described below.

Step 1: Initialize S_{opt} as an empty set.

Step 2: For all test points corresponding to fault pairs with $NT_i = 1$, add these test points to S_{opt} . Remove from the Boolean table any fault pairs that these test points can isolate, and then delete these test points from the table. Proceed to Step 4.

Step 3: For $NT_i = NT_i + 1$, calculate the $NI(t_j)$ values for all remaining test points in the fault pair Boolean table. Add the test point t_j with the largest $NI(t_j)$ value to S_{opt} . Remove from the table the fault pairs that the test point t_j can isolate, and then delete that test point from the Boolean table.

Step 4: The algorithm terminates if all fault pairs are isolated or no further fault pairs can be isolated. If not, return to Step 3.

4.2. Algorithm time complexity analysis

In this section, the computational complexity of the proposed algorithm is discussed in detail as follows:

1. For each fault's test data, KDE is used to estimate its distribution, while GWO optimizes the bandwidth parameter of KDE. Here, k represents the number of faults, n is the number of test points, m is the number of fault samples per test point, W denotes the number of grey wolves, and T is the maximum number of iterations. The overall computational complexity is $O(k \cdot n \cdot T \cdot W \cdot m)$.
2. After estimating the data distribution of each fault across different test points, Equations (4) and (5) are used to compute the distribution overlap, thereby constructing the fault-pair Boolean table. Since $k \cdot (k - 1)/2$ fault pairs need to be evaluated, the overall computational complexity is $O(k \cdot (k - 1)/2) = O(k^2)$.
3. In Step 2 of the algorithm in Section 4.1, it is necessary to search for rows where $NT_i = 1$ in each fault pair. Thus, the overall computational complexity is $O(k \cdot (k - 1)/2) = O(k^2)$.
4. In Step 3 of the algorithm in Section 4.1, since it is necessary to search for $NI(t_j)$ within the $k \cdot (k - 1)/2$ rows and n columns of fault-pair isolation table, the computational complexity is $O(n \cdot k \cdot (k - 1)/2) = O(n \cdot k^2)$.

If Step 3 is executed N times, the overall algorithm complexity is $O(k \cdot n \cdot T \cdot W \cdot m + 2k^2 + N \cdot n \cdot k^2) = O(k \cdot n \cdot T \cdot W \cdot m + N \cdot n \cdot k^2)$.

5. CASE STUDY

In this section, negative feedback circuit (NFC) and active filter circuit (AFC) are used to verify the validity of the proposed method.

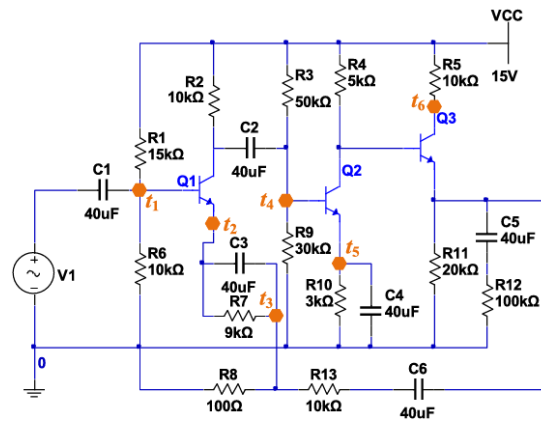


Figure 2. NFC schematic diagram. NFC: Negative feedback circuit.

Table 1. Fault types of the NFC

Fault type	Fault mode
f_1	Q_1 B–C short
f_2	Q_1 C–E short
f_3	Q_2 C–E short
f_4	$R_8 = 130\Omega$
f_5	$R_9 = 39k\Omega$
f_6	Q_1 B–C short & Q_2 C–E short
f_7	Q_1 C–E short & $R_8 = 130\Omega$
f_8	Q_1 C–E short & $R_9 = 39k\Omega$
f_9	Q_1 B–C short & $R_8 = 130\Omega$ & $R_9 = 39k\Omega$
f_{10}	Q_1 C–E short & $R_8 = 130\Omega$ & $R_9 = 39k\Omega$

NFC: Negative feedback circuit.

5.1. Experiment on NFC

The NFC feeds the output signal back to the input signal in proportion to the controller in a robotic system. This feedback mechanism enables the system to dynamically adjust its behavior by comparing the actual output with the desired input, thereby minimizing errors and enhancing performance. Studying the test point selection for NFC is essential to ensure the robotic system's reliability, efficiency, and fault tolerance^[29]. The schematic diagram of the NFC is given in Figure 2.

As illustrated in Figure 2, the input signal is a sinusoidal wave with a frequency of 1 kHz and an amplitude of 7 mV. The supply voltage is set to 15 V, and the tolerances of the resistors and capacitors are set at 5%. Data collection is performed using six test points $T = \{t_1, t_2, t_3, t_4, t_5, t_6\}$. Additionally, as presented in Table 1, ten fault types are employed for experimental validation.

5.1.1. Experimental results of the proposed method

A total of 10^3 test data samples are collected for each fault type using the Monte Carlo method from six test points. In this study, the threshold is set to $\varepsilon = 0.95$ ^[30]. By traversing all fault types and test points, the fault-pair Boolean table is constructed using the BC and KDE methods, as given in Table 2.

According to Table 2, considering the fault-pair isolation results, test points t_1 and t_2 are initially added to the optimal test point set S_{opt} due to their ability to isolate key fault pairs effectively. Subsequently, the fault pairs

Table 2. Fault-pair Boolean tables based on BC

No.	Fault pair	t_1	t_2	t_3	t_4	t_5	t_6	NT_i
1	(f_0, f_1)	0	1	0	0	0	0	1
2	(f_0, f_2)	0	1	0	0	0	0	1
⋮	⋮	⋮	⋮	⋮	⋮	⋮	⋮	⋮
11	(f_1, f_2)	1	0	0	0	0	0	1
⋮	⋮	⋮	⋮	⋮	⋮	⋮	⋮	⋮
20	(f_2, f_3)	0	1	0	0	0	1	2
⋮	⋮	⋮	⋮	⋮	⋮	⋮	⋮	⋮
28	(f_3, f_4)	0	1	0	0	1	0	2
⋮	⋮	⋮	⋮	⋮	⋮	⋮	⋮	⋮
35	(f_4, f_5)	0	1	0	0	0	0	1
⋮	⋮	⋮	⋮	⋮	⋮	⋮	⋮	⋮
41	(f_5, f_6)	0	1	0	1	1	0	3
⋮	⋮	⋮	⋮	⋮	⋮	⋮	⋮	⋮
46	(f_6, f_7)	1	0	0	0	1	0	2
⋮	⋮	⋮	⋮	⋮	⋮	⋮	⋮	⋮
50	(f_7, f_8)	0	1	0	0	0	0	1
⋮	⋮	⋮	⋮	⋮	⋮	⋮	⋮	⋮
55	(f_9, f_{10})	1	0	0	1	1	0	3
	$NI(t_i)$	14	41	0	8	19	8	-

BC: Bhattacharyya coefficient.

that can be isolated by t_1 and t_2 are eliminated from further consideration. After completing this process, it is observed that all fault pairs are successfully isolated. Therefore, t_1 and t_2 are identified as the optimal test points for the NFC system, ensuring accurate and efficient fault isolation.

5.1.2. Comparison results of the test points selection

Comparisons are made with two types of fault-pair tables presented in [19] and [20], both of which assume that the data follows a normal distribution. Additionally, [19] further requires calculations to be performed within a specified range $[u_i - w \cdot \sigma_i, u_i + w \cdot \sigma_i]$, where the value of w influences the precision of the results. In this study, thresholds of $\varepsilon = 0.95$ and $\varepsilon = 0.98$ are selected for comparison. To evaluate the effectiveness of GWO in optimizing the kernel bandwidth, a comparison is also made with the results obtained using particle swarm optimization for kernel bandwidth optimization (PSO-KDE). The detailed results are presented in Table 3.

In Table 3, the column labeled S_{opt} represents the optimal set of test points. The fourth column indicates the fault isolation degree, which refers to the total number of faults that can be fully isolated using the selected optimal test points. The final column shows the number of faults pairs that cannot be isolated. The test point selection performance is compared under two thresholds ($\varepsilon = 0.95$ and $\varepsilon = 0.98$). For $\varepsilon = 0.95$, test points t_3 and t_4 are selected in [19] under different w values yield a fault isolation degree of 4, with 7, 7, and 8 remaining fault pairs, respectively, indicating limited isolation performance. In contrast, the test points selected t_2, t_3, t_4 in [20] achieve a fault isolation degree of 7, reducing the number of remaining fault pairs to 2. Both the PSO-KDE

Table 3. Comparison results of the proposed method with the methods in [19] and [20]

	Method	S_{opt}	Fault isolation	Number of remainder
			degree	fault pairs
$\varepsilon = 0.95$	[19] ($w = 1.96$)	t_3, t_4	4	7
	[19] ($w = 2.576$)	t_3, t_4	4	7
	[19] ($w = 3$)	t_3, t_4	4	8
	[20]	t_2, t_3, t_4	7	2
	PSO-KDE	t_1, t_2	11	-
	The proposed method	t_1, t_2	11	-
$\varepsilon = 0.98$	[19] ($w = 1.96$)	-	-	55
	[19] ($w = 2.576$)	t_3, t_4	4	8
	[19] ($w = 3$)	t_3, t_4	4	8
	[20]	t_2, t_3, t_4	7	2
	PSO-KDE	t_1, t_2, t_5	11	-
	The proposed method	t_1, t_2	11	-

PSO-KDE: Particle swarm optimization for kernel bandwidth optimization.

algorithm and the proposed method select test points t_1 and t_2 , achieving the highest fault isolation degree of 11 with zero remaining fault pairs, demonstrating superior performance.

For the threshold $\varepsilon = 0.98$, [19] selects the same test points as for $\varepsilon = 0.95$, maintaining a fault isolation degree of 4 with 55, 8, and 8 remaining fault pairs, respectively. Similarly, t_2, t_3, t_4 are selected in [20] achieving a fault isolation degree of 7 with two remaining fault pairs. The proposed method selects the test points t_1, t_2 once again, achieving the highest fault isolation degree of 11 with zero remaining fault pairs, demonstrating a best performance. Although the PSO-KDE method can also achieve the highest fault isolation degree of 11 with zero remaining fault pairs, it selects three test points t_1, t_2, t_5 , which is more than the number of test points required by the proposed method.

In summary, the proposed method consistently achieved complete fault isolation across different thresholds, while selecting the fewest test points. It significantly outperformed the methods in [19] and [20], and PSO-KDE, demonstrating its superior fault isolation capability and adaptability.

5.2. Experiment on AFC

The AFC can filter and purify signals in robotic systems, eliminating noise interference and providing high-precision feedback signals for the controller. It can also monitor and control the current in the motor drive circuits in real-time, ensuring the stability and accuracy of the motor current, preventing abnormal motor operation or damage caused by excessive or insufficient current. This improves the control precision and operational efficiency of the motor, enabling precise control of robot movements. The schematic diagram of the AFC is given in Figure 3.

In the AFC circuit, the tolerance of resistors and capacitors is set to 5% and 10%, respectively. The second circuit experiment mainly simulates hard faults in the circuit. A total of 19 hard faults were simulated, and ten test points (t_1 to t_{10}) were used to collect fault data. The fault modes are shown in Table 4.

A total of 10^3 test data samples are collected for each fault type using the Monte Carlo method from ten test points. Based on the collected data, a fault pair Boolean table is constructed and used to perform optimal test point selection. As in Section 5.1, the proposed method is compared with the methods in [19] and [20]. In the

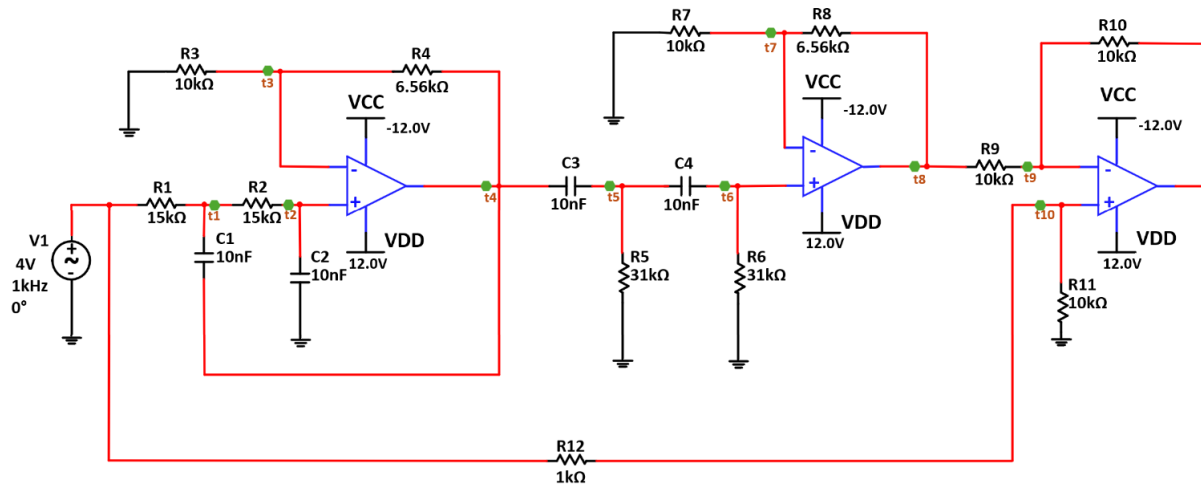


Figure 3. AFC schematic diagram. AFC: Active filter circuit.

Table 4. Fault types of the AFC

Fault type	Fault mode	Fault type	Fault mode
f_0	Normal	f_{10}	R_7 open
f_1	R_1 short	f_{11}	R_8 open
f_2	R_1 open	f_{12}	R_9 open
f_3	R_2 short	f_{13}	R_{10} open
f_4	R_2 open	f_{14}	R_{11} open
f_5	R_3 open	f_{15}	R_{12} open
f_6	R_5 short	f_{16}	C_1 open
f_7	R_5 open	f_{17}	C_2 open
f_8	R_6 short	f_{18}	C_3 open
f_9	R_6 open	f_{19}	C_4 open

AFC: Active filter circuit.

experiment, thresholds $\varepsilon = 0.95$ and $\varepsilon = 0.98$ are selected to determine whether two faults can be isolated. To evaluate the effectiveness of GWO in optimizing the kernel bandwidth, a comparison is also made with the results obtained using PSO-KDE. The simulation and comparison results are presented in Table 5.

In Table 5, the test point selection performance is compared under two thresholds ($\varepsilon = 0.95$ and $\varepsilon = 0.98$). For $\varepsilon = 0.95$, test points $t_3, t_4, t_7, t_8, t_9, t_{10}$ are selected in [19] under different w values yield a fault isolation degree of 7, 7, and 9, with 74, 74, and 68 remaining fault pairs, respectively, indicating limited isolation performance. In contrast, the test points selected $t_3, t_4, t_7, t_9, t_{10}$ in [20] achieve a fault isolation degree of 13, reducing the number of remaining fault pairs to 20. Both the PSO-KDE algorithm and the proposed method select test points t_1, t_2, t_3, t_4 and t_1, t_2, t_3, t_4 , achieving the highest fault isolation degree of 16 with six remaining fault pairs, demonstrating superior performance.

For the threshold $\varepsilon = 0.98$, [19] selects the same test points as for $\varepsilon = 0.95$, maintaining a fault isolation degree of 7 with 190, 74, and 74 remaining fault pairs, respectively. Similarly, $t_3, t_4, t_7, t_9, t_{10}$ are selected in [20] achieving a fault isolation degree of 13 with 20 remaining fault pairs. The proposed method selects the test points t_1, t_2, t_3, t_4 once again, achieving the highest fault isolation degree of 16 with six remaining fault pairs, demonstrating a best performance. Although the PSO-KDE algorithm and the proposed method select test points t_1, t_2, t_3, t_4 and t_1, t_2, t_3, t_4 , both achieve the highest fault isolation degree of 16 with six remaining fault pairs, demonstrating superior performance.

Table 5. Comparison results of the proposed method with the methods in [19] and [20]

	Method	S_{opt}	Fault isolation degree	Number of remainder fault pairs
$\varepsilon = 0.95$	[19] ($w = 1.96$)	$t_3, t_4, t_7, t_8, t_9, t_{10}$	7	74
	[19] ($w = 2.576$)	$t_3, t_4, t_7, t_8, t_9, t_{10}$	7	74
	[19] ($w = 3$)	$t_3, t_4, t_7, t_8, t_9, t_{10}$	9	68
	[20]	$t_3, t_4, t_7, t_9, t_{10}$	13	20
	PSO-KDE	t_1, t_2, t_3, t_4	16	6
	The proposed method	t_1, t_2, t_3, t_4	16	6
$\varepsilon = 0.98$	[19] ($w = 1.96$)	-	-	190
	[19] ($w = 2.576$)	$t_3, t_4, t_7, t_8, t_9, t_{10}$	7	74
	[19] ($w = 3$)	$t_3, t_4, t_7, t_8, t_9, t_{10}$	7	74
	[20]	$t_3, t_4, t_7, t_9, t_{10}$	13	20
	PSO-KDE	t_1, t_2, t_3, t_4	16	6
	The proposed method	t_1, t_2, t_3, t_4	16	6

PSO-KDE: Particle swarm optimization for kernel bandwidth optimization.

In summary, it can be seen from the above two circuit case studies that the proposed method isolates the maximum number of faults at different thresholds while selecting the minimum number of test points. It significantly outperformed the methods in [19] and [20], and PSO-KDE, demonstrating its superior fault isolation capability and adaptability.

6. CONCLUSIONS

This paper has presented a novel test point selection method that extends the fault-pair Boolean table into a distribution-based framework. By integrating BC to quantify distributional overlap and KDE to model circuit response distributions without normal distribution assumptions, the method has effectively improved test point selection. The GWO algorithm has been employed to optimize the bandwidth parameter in KDE, ensuring accurate estimation. Experimental results on a NFC have demonstrated that the proposed method consistently achieves the highest fault isolation degree of 11 with zero remaining fault pairs, even under different thresholds ($\varepsilon = 0.95$ and $\varepsilon = 0.98$). Furthermore, the experimental results further show that the method on the AFC consistently achieves the highest fault isolation degree of 16 with six remaining fault pairs under different thresholds ($\varepsilon = 0.95$ and $\varepsilon = 0.98$). In contrast, traditional methods in [19] and [20] resulted in multiple unresolved fault pairs. These findings confirm the superior accuracy, adaptability, and efficiency of the proposed method, making it highly suitable for fault isolation in analog circuits.

However, there are still several areas that warrant further exploration for fault-pair Boolean tables. As robotic systems are dynamic and subject to frequent changes in operational conditions, it is crucial to develop adaptive fault-pair Boolean tables that can update in real-time as new fault data is collected. Another important direction for future research is the integration of uncertainty modeling into fault-pair Boolean tables, as real-world fault data is often noisy and incomplete.

DECLARATIONS

Authors' contributions

Supervision, project administration, writing - review and editing: Wang, X.

Methodology, analysis and interpretation of data, writing - original draft, software: Xie, D.

Supervision, conceptualization, project administration, writing - review and editing: Li, Y.

Writing - review and editing, supervision: Tian, J.; Li, K.

Availability of data and materials

The original contributions presented in the study are included in the article; further inquiries can be directed to the corresponding author.

Financial support and sponsorship

This work was supported by the National Natural Science Foundation of China (Nos.62303293, 62303414), the China Postdoctoral Science Foundation (Nos. 2023M732176, 2023M741821) and the Zhejiang Province Postdoctoral Selected Foundation (No. ZJ2023143).

Conflicts of interest

The author Li, K. in this article is affiliated with Jiaxing New Jies Heat & Power Co., Ltd., while other authors declare that there are no conflicts of interest.

Ethical approval and consent to participate

Not applicable.

Consent for publication

Not applicable.

Copyright

© The Author(s) 2025.

REFERENCES

1. Chen, H.; Liu, Z.; Alippi, C.; Huang, B.; Liu, D. Explainable intelligent fault diagnosis for nonlinear dynamic systems: from unsupervised to supervised learning. *IEEE Trans. Neural Netw. Learn. Syst.* **2022**, *35*, 6166–79. [DOI](#)
2. Chen, H.; Jiang, B.; Ding, S. X.; Huang, B. Data-driven fault diagnosis for traction systems in high-speed trains: a survey, challenges, and perspectives. *IEEE Trans. Intell. Transp. Syst.* **2020**, *23*, 1700–16. [DOI](#)
3. Arabi, A.; Ayad, M.; Bourouba, N.; et al. An efficient method for faults diagnosis in analog circuits based on machine learning classifiers. *Alex. Eng. J.* **2023**, *77*, 109–25. [DOI](#)
4. Wang, S.; Jia, Z.; Liu, Z.; Tang, Y.; Qin, X.; Wang, X. Self-supervised contrast learning based UAV fault detection and interpretation with spatial–temporal information of multivariate flight data. *Expert Syst. Appl.* **2025**, *267*, 126156. [DOI](#)
5. Piccirilli, M. C.; Luchetta, A. Diagnosis in analog electronic circuits, electrical power systems and smart grids. *Electronics* **2022**, *11*, 2008. [DOI](#)
6. Abo-elftooh, B. A.; El-Mahlawy, M. H.; Ragai, H. F. New digital testing for parametric fault detection in analog circuits using classified frequency-bands and efficient test-point selection. *Ain Shams Eng. J.* **2021**, *12*, 1701–21. [DOI](#)
7. Starzyk, J. A.; Liu, D.; Liu, Z. H.; Nelson, D. E.; Rutkowski, J. O. Entropy-based optimum test points selection for analog fault dictionary techniques. *IEEE Trans. Instrum. Meas.* **2004**, *53*, 754–61. [DOI](#)
8. Yang, C.; Tian, S.; Long, B.; Chen, F. Methods of handling the tolerance and test-point selection problem for analog-circuit fault diagnosis. *IEEE Trans. Instrum. Meas.* **2011**, *60*, 176–85. [DOI](#)
9. Yang, C.; Tian, S.; Long, B.; Chen, F. A test points selection method for analog fault dictionary techniques. *Analog Integr. Circ. Sig. Process.* **2010**, *63*, 349–57. [DOI](#)
10. Gao, Y.; Yang, C.; Tian, S.; Chen, F. Entropy based test point evaluation and selection method for analog circuit fault diagnosis. *Math. Probl. Eng.* **2014**, *2014*, 259430. [DOI](#)
11. Cui, Y.; Shi, J.; Wang, Z. Analog circuit test point selection incorporating discretization-based fuzzification and extended fault dictionary to handle component tolerances. *J. Electron. Test.* **2016**, *32*, 661–79. [DOI](#)
12. Ye, X.; Chen, C.; Zhai, G. Fault localization of a switched mode power supply based on extended integer-coded dictionary method. *Microelectron. Reliab.* **2018**, *88–90*, 339–44. [DOI](#)
13. Saeedi, S.; Pishgar, S. H.; Eslami, M. Optimum test point selection method for analog fault dictionary techniques. *Analog Integr. Circ. Sig. Process.* **2019**, *100*, 167–79. [DOI](#)
14. Yang, C.; Tian, S.; Long, B.; Chen, F. A novel test point selection method for analog fault dictionary techniques. *J. Electron. Test.* **2010**, *26*, 523–34. [DOI](#)
15. Tian, S.; Yang, C.; Long, B. Selection of minimal test points set for integer-coded fault wise table. In *2009 IEEE Circuits and Systems*

- International Conference on Testing and Diagnosis*, Chengdu, China. Apr 28–29, 2009. IEEE; 2009. pp. 312–6. [DOI](#)
16. Prasad, V. C.; Pinjala, S. N. R. A fast algorithm for the generation of fault dictionary of linear analog circuits using adjoint network approach. In *1990 IEEE International Symposium on Circuits and Systems (ISCAS)*, New Orleans, USA. May 01–03, 1990. IEEE; 1990. pp. 37–40. [DOI](#)
 17. Luo, H.; Wang, Y.; Lin, H.; Jiang, Y. A new optimal test node selection method for analog circuit. *J. Electron. Test.* **2012**, *28*, 279–90. [DOI](#)
 18. Tang, X.; Xu, A. Practical analog circuit diagnosis based on fault features with minimum ambiguities. *J. Electron. Test.* **2016**, *32*, 83–95. [DOI](#)
 19. Zhao, D.; He, Y. A new test point selection method for analog circuit. *J. Electron. Test.* **2015**, *31*, 53–66. [DOI](#)
 20. Ma, Q.; He, Y.; Zhou, F.; Song, P. Test point selection method for analog circuit fault diagnosis based on similarity coefficient. *Math. Probl. Eng.* **2018**, *2018*, 9714206. [DOI](#)
 21. Yang, B.; Lei, Y.; Li, X.; Li, N. Targeted transfer learning through distribution barycenter medium for intelligent fault diagnosis of machines with data decentralization. *Expert Syst. Appl.* **2024**, *244*, 122997. [DOI](#)
 22. Van Molle, P.; Verbelen, T.; Vankeirsbilck, B.; et al. Leveraging the Bhattacharyya coefficient for uncertainty quantification in deep neural networks. *Neural Comput. Appl.* **2021**, *33*, 10259–75. [DOI](#)
 23. Lu, J.; Yue, J.; Zhu, L.; Li, G. Variational mode decomposition denoising combined with improved Bhattacharyya distance. *Measurement* **2020**, *151*, 107283. [DOI](#)
 24. Kitahara, M.; Bi, S.; Broggi, M.; Beer, M. Nonparametric Bayesian stochastic model updating with hybrid uncertainties. *Mech. Syst. Signal Process.* **2022**, *163*, 108195. [DOI](#)
 25. Tang, X.; Xu, A.; Niu, S. KKCVCV-GA-based method for optimal analog test point selection. *IEEE Trans. Instrum. Meas.* **2016**, *66*, 24–32. [DOI](#)
 26. Wu, Y.; Liu, X.; Wang, Y. L.; Li, Q.; Guo, Z.; Jiang, Y. Improved deep PCA and Kullback–Leibler divergence based incipient fault detection and isolation of high-speed railway traction devices. *Sustain. Energy Technol. Assess.* **2023**, *57*, 103208. [DOI](#)
 27. Pan, J.; Zou, Z.; Sun, S.; Su, Y.; Zhu, H. Research on output distribution modeling of photovoltaic modules based on kernel density estimation method and its application in anomaly identification. *Sol. Energy* **2022**, *235*, 1–11. [DOI](#)
 28. Yu, X.; Jiang, N.; Wang, X.; Li, M. A hybrid algorithm based on grey wolf optimizer and differential evolution for UAV path planning. *Expert Syst. Appl.* **2023**, *215*, 119327. [DOI](#)
 29. Li, Y.; Chen, H.; Lu, N.; Jiang, B.; Zio, E. Data-driven optimal test selection design for fault detection and isolation based on CCVKL method and PSO. *IEEE Trans. Instrum. Meas.* **2022**, *71*, 1–10. [DOI](#)
 30. Alangari, N.; Menai, M. E. B.; Mathkour, H.; Almosallam, I. Intrinsically interpretable Gaussian mixture model. *Information* **2023**, *14*, 164. [DOI](#)